The Journal of Experimental Biology 207, 2835-2844
Published by The Company of Biologists 2004
doi:10.1242/jeb.01089

Extracellular H^+ dynamics during oogenesis in *Rhodnius prolixus* ovarioles

C. S. Bjornsson[1] and E. Huebner[2,*]

[1]*Laboratory of Nervous System Disorders, Wadsworth Center, Albany, NY 12201-0509, USA* and
[2]*Department of Zoology, University of Manitoba, Winnipeg, MB, Canada R3T 2N2*

*Author for correspondence (e-mail: ehuebnr@cc.umanitoba.ca)

Accepted 18 May 2004

Summary

The spatiotemporal dynamics of transmembrane hydrogen ion (H^+) fluxes during oogenesis were investigated in the telotrophic ovarioles of the insect, *Rhodnius prolixus*. Although *Rhodnius* ovarioles possess exaggerated morphological and electrical polarity between nurse cells and oocytes, little is known about H^+ changes during oogenesis, despite the regulatory role played by H^+ and pH in many relevant cellular processes. A number of dynamic extracellular H^+ fluxes were measured along *Rhodnius* ovarioles, representing an oogenesis cycle, using a non-invasive, self-referencing, H^+-selective probe. The interfollicular stalk separating adjacent follicles exhibited prominent H^+ efflux that peaked during midvitellogenesis and declined during late vitellogenesis. H^+ efflux in this region preceded stalk formation and, importantly, preceded the onset of vitellogenesis in the adjacent posterior follicle. H^+ efflux was also observed over the terminal follicle, where specialized regions of the chorion were forming, and was still detected around follicle cells after ovulation, indicating that the somatic follicular epithelium produced this flux. Transmembrane H^+ fluxes may drive intracellular pH changes or may stabilize pH_i in response to pH-altering events. H^+ fluxes may play a role in processes that coincide spatially and temporally, including the onset of vitellogenesis, endocytosis, follicle cell cytoskeletal dynamics, and regulation of interfollicular feedback mechanisms.

Key words: hydrogen, H^+, ion-selective probe, oogenesis, insect, *Rhodnius prolixus.*

Introduction

The egg is a truly remarkable cell that not only stockpiles enough synthetic material to last the future embryo through early development, but also contains maternal determinants necessary to establish the blueprint for the future organism. In insect meroistic ovarioles, most of these products are prepared by nurse cells for subsequent transport to the oocyte *via* cytoplasmic bridges (Vanderberg, 1963; Huebner, 1981a; Huebner and Anderson, 1972c; Gutzeit, 1986). Yolk products, synthesized by the fat body and ovarian follicle cells, are actively endocytosed by vitellogenic oocytes following activation of the previtellogenic oocyte (Telfer, 1965, 1975). Nurse cells and oocytes retain cytoplasmic continuity after undergoing incomplete cell divisions (Lutz and Huebner, 1980, 1981), but differ in their transcriptional and synthetic activity (Telfer, 1975), cytoskeletal dynamics (Huebner, 1984; Gutzeit and Huebner, 1986), cell membrane activity and bioelectrical properties (Woodruff et al., 1986a; Woodruff and Telfer, 1990; O'Donnell and Sharda, 1994). In particular, differences in intracellular ion activity can impact a broad spectrum of cellular functions relevant to oogenesis. Alterations in intracellular pH (pH_i) can coordinate changes in metabolic activity (reviewed by Busa and Nuccitelli, 1984), microtubule and F-actin assembly and dynamics (Tilney et al., 1978; Regula et al., 1981; Schatten et al., 1985; Southwick, 2000), and gap junctional coupling (Perrachia and Perrachia, 1980; Bohrmann and Haas-Assenbaum, 1993; Francis et al., 1999; Anderson and Woodruff, 2001). During insect oogenesis, vesicular acidification is required for subsequent processing of the endosomal compartments in several species (Dittmann, 1997; Dittmann and Munz, 1999; Nordin et al., 1990, 1991; Woodruff and Telfer, 2002). In the polytrophic ovarioles of *Hyalophora cecropia*, a rise in pH_i is accompanied by a range of physiological changes at the onset of vitellogenesis (Woodruff and Telfer, 1990), suggesting that pH_i change may increase oocyte metabolic activity. In *Rhodnius* oocytes, membrane potential and pH_i are affected by extracellular pH changes (O'Donnell and Sharda, 1994).

Insect cells commonly harness electrogenic H^+ transport to help maintain membrane potential and to produce a transmembrane chemical gradient that drives secondary transport mechanisms (Dittmann, 1997; Haley and O'Donnell, 1997; Harvey and Wieczorek, 1997). The dependence of cellular H^+ regulation on the extracellular space makes this ion ideally suited to investigation using a self-referencing, extracellular, ion-selective probe (ISP), permitting selective H^+ measurement with minimal perturbation of the tissue. Previous studies using extracellular voltage-sensitive probes have established that dynamic bioelectric currents are present

around ovarioles of a number of insects (Bohrmann et al., 1986; Bowdan and Kunkel, 1990, 1994; Diehl-Jones and Huebner, 1989, 1992; Dittmann et al., 1981; Huebner and Sigurdson, 1986; Jaffe and Woodruff, 1979; Overall and Jaffe, 1985; Verachtert and DeLoof, 1986; Woodruff et al., 1986b). Ion substitution studies and exposure to pharmacological agents have demonstrated that Na^+, Cl^-, K^+ and Ca^{2+} contribute to these currents in *Rhodnius* (Diehl-Jones and Huebner, 1993). Although voltage-sensitive probes have provided some insight into the character of these ionic currents they are inherently limited, since current alterations due to secondary or synergistic effects of pharmacological perturbation are difficult to rule out. The ion-selective probe offers a considerable advantage as a direct measuring tool without pharmacological complications.

The telotrophic ovarioles of *Rhodnius prolixus* provide an ideal model for this study, since they possess an exaggerated polarity between nurse cells and oocytes, and there exists a wealth of morphological, endocrinological and electrophysiological data. The coupling of oogenesis to the ingestion of a blood meal also makes identification of causal relationships more likely. Despite the importance of pH in many cell processes relevant to oogenesis in *Rhodnius*, little is known about pH and H^+ flux during this process. O'Donnell and Sharda (1994) determined the pH_i of vitellogenic follicles 400–600 μm in length and carefully investigated the pH-dependence of oocyte membrane potential, but did not examine H^+ flux and pH changes related to oocyte growth over a complete oogenesis cycle. Determining the timing and magnitude of extracellular H^+ dynamics is an essential first step towards understanding the potential role(s) of transmembrane fluxes during oogenesis. By determining the spatial and temporal distribution of H^+ fluxes around the ovariole during a complete oogenesis cycle, we can gain insight into regional and stage-specific pH_i changes in the adult *Rhodnius* ovariole, and can consider these in relation to the cell differentiation and regulatory events of oogenesis.

Materials and methods

Ovariole preparation

A colony of *Rhodnius prolixus* Stahl was maintained at 27°C and 65% relative humidity, and fed every 3–4 weeks on rabbits or using an artificial membrane technique (Huebner et al., 1994). Ovaries dissected from mated adult females 3–12 days post feed (d.p.f.) were transferred to Petri dishes containing modified O'Donnell's *Rhodnius* Ringers (O'Donnell, 1985), composed of 129 mmol l^{-1} NaCl, 8.6 mmol l^{-1} KCl, 0.02 mmol l^{-1} $CaCl_2$, 10.48 mmol l^{-1} $MgCl_2$, 48 mmol l^{-1} dextrose and 1 mmol l^{-1} Hepes, pH 7.0, adjusted to 340 mOsm with glucose. Ovarioles were carefully isolated and desheathed using jeweler's tweezers and sharpened tungsten needles. The reduced Hepes concentration minimized dampening of H^+ fluxes (Kunkel and Faszewski, 1995). Mg^{2+} was added to compensate for the reduced [Ca^{2+}], and osmolarity was adjusted using glucose. Ovarioles under these conditions behaved normally: muscular contractions of the ovariole sheaths appeared to be unaffected over the time period needed to complete a scan. Ovarioles were transferred to a customised recording chamber that minimized deformation and stretching (Bjornsson and Huebner, 2002). Ovarioles were staged based on terminal (T) follicle length (Pratt and Davey, 1972), as shown in Table 1.

Table 1. *Ovariole stages spanning an oogenesis cycle in* Rhodnius

Stage	T oocyte length (μm)	Differentiation features
1	300–400	Late previtellogenesis
2	400–500	Onset of vitellogenesis
3	500–600	Early vitellogenesis
4	600–700	Early vitellogenesis
5	700–800	Midvitellogenesis
6	800–900	Mid-late vitellogenesis
7	900–1000	Late vitellogenesis
8	1000–1500	NC-oocyte continuity lost (trophic cord closes)
9	1500–2000	Chorionation

Staging was based on T follicle length, and characterized by specific developmental events, listed here.

Ion-selective probe (ISP) technique

Extracellular H^+ flux was measured with the automated scanning electrode technique (ASET) using a non-invasive ion-selective probe (ISP; Applicable Electronics, Inc., Sandwich, MA, USA; Science Wares, Inc., Falmouth, MA, USA) based on Kuhtreiber and Jaffe (1990) and Somieski and Nagel (2001). Glass electrodes were fashioned from TW150-4 borosilicate capillary tubes (World Precision Instruments, Inc., Sarasota, FL, USA) pulled to a 4 μm diameter tip on a Sutter P-97 Flaming/Brown pipette puller (Novato, CA, USA). Batches of 30–40 electrodes were preheated overnight at 200°C in a presilanized 100 ml glass chamber, silanized by adding 80 μl dichlorosilane (Sigma-Aldrich, St Louis, MO, USA) to the chamber for 30 min, and postsilanized overnight at 200°C after the chamber was briefly vented (A. Shipley and J. Kunkel, personal communication). H^+ probes were backfilled with 40 mmol l^{-1} KH_2PO_4 and 100 mmol l^{-1} KCl, pH 7.0, then frontfilled with a 40–50 μm column of hydrogen liquid ion exchanger (#85293, Fluka Chemie, Inc., Switzerland). The H^+ probe was placed in an electrode holder (#MEH2SW15, World Precision Instruments, Sarasota, FL. USA) with an Ag/AgCl wire. A DRIREF2 (World Precision Instruments) was used as a reference electrode. The ASET preamplifiers and 3D stepper motor system were mounted on a Zeiss IM35 microscope (Zeiss Canada, Toronto) using a modified stage.

x–y axes transmitted images of the ovariole were acquired using a Zeiss plan 2.5× objective and a Cohu 6500 (San Diego, CA, USA) video camera. Side view (*z*-axis) images were captured using a Panasonic WV-CD50 video camera fitted with

a long focal length Optem Zoom-70 lens (Thales Optern, Fairport, NY, USA). A Computer Eyes 1024 framegrabber (Digital Vision Inc.) received inputs from both cameras. A Fostec (Schott-Fostec, Southbridge, MA, USA) fiber-optic lamp fitted with an infrared filter illuminated the sample. A Melles Griot (Ottawa, Canada) air table was used to minimize vibrations, and a Faraday cage (built by the authors) was used to minimize external electronic interference. The ISP signal was independently monitored using a Tektronics 2205 oscilloscope (Beaverton, OR, USA) to evaluate probe noise. All ISP and peripheral equipment was connected to a dedicated AC wall outlet with a neutral line connected directly to ground through an isolation transformer to eliminate noise from other equipment in the building; this arrangement was of utmost importance to achieve the low noise necessary to detect ion fluxes at the biological level.

Electrode calibrations were performed at the beginning and end of each ovariole scan, by measuring voltage offset in 0.1 mol l^{-1} phosphate buffers with pH 8.0, 7.0 and 6.0, providing a measure of the probe's accuracy and response speed. H^+-selective probes were only used if the slope of a line derived by plotting the logarithm of $[H^+]$ *vs.* the electrode's voltage output equaled the expected Nernst value of 56.2 mV (±5%) per tenfold change in concentration, and the probe took less than 10 s to settle on a voltage value during the calibration procedure at the beginning and end of each ovariole scan.

Each scan included background noise measurements taken at a point over 500 μm away from the tissue before and after scanning points along the ovariole. Twenty-five positions were measured along all stage 2–9 ovarioles (Fig. 1); additional positions measured in some ovarioles were included to obtain more information as the stalk separating T and T-1 follicles formed, as follicle cells began to differentiate during stages 2–3, and also to measure specific areas associated with the development of regionally specialized chorion production during stages 8–9. In some cases, certain positions did not exist or were inaccessible without severe disruption of the tissue and recording chamber; measurements were not made at these points. An image was captured at every point measured, to record the probe's position, to allow proper placement of a vector representing the H^+ flux at that point during data analysis (described below), and to permit assessment of the ovariole's condition throughout the scan.

A 3-D sampling routine was used to measure H^+ concentration at an 'origin' position within 2 μm of the ovariole surface, and 10 μm away from this origin in each of the *x*- and *y*-axes in the horizontal plane, and in the vertical *z*-axes, for a total of four measurements (Fig. 2). At each of these four points, the probe was paused for 1 s before taking a 1 s reading. Five complete 3-D measurements were taken at each position along the ovariole, and averaged during analysis. All positions were measured halfway up the ovariole in the vertical *z*-axis.

Exported data were compiled using Microsoft Excel™, where H^+ flux was calculated based on the method of Kuhtreiber and Jaffe (1990). The equations used to calculate

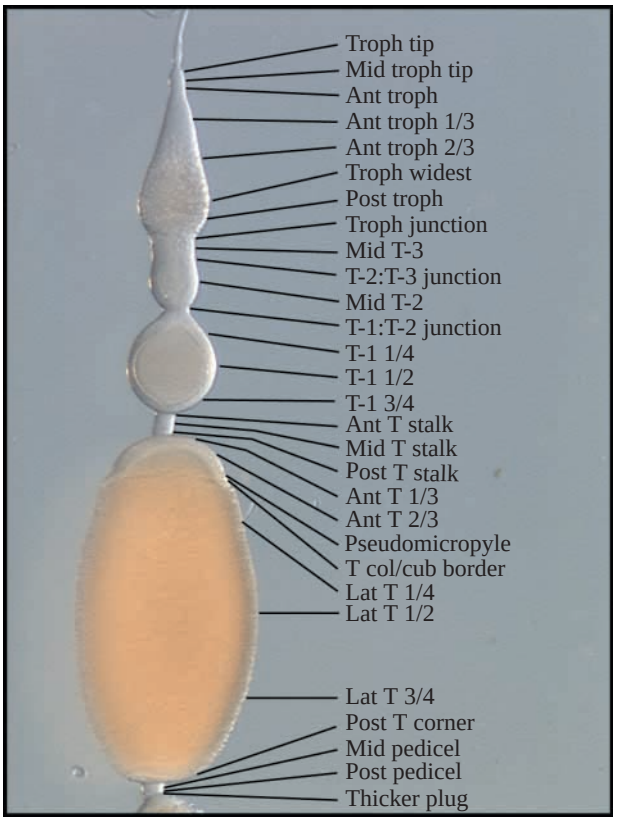

Fig. 1. An illustration depicting the positions along adult ovarioles of different stages measured during a scan. As the connective stalk (see stage 4) and the anterior region of the T and T-1 follicle (stages 8–9) became more complex, additional points were introduced to include measurements of these dynamic and potentially interesting regions.

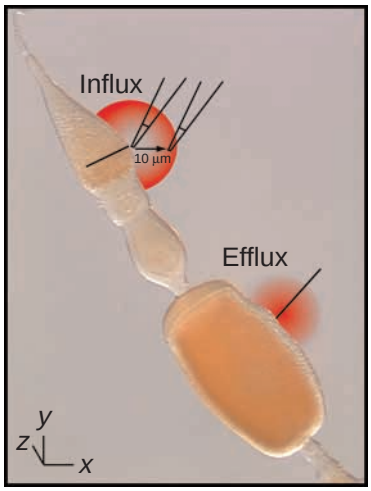

Fig. 2. Examples of H^+ influx and efflux. 2-D vectors were calculated from measurements taken near the ovariole and 10 μm away in the *x*- and *y*-axis, and superimposed over an image of the ovariole. Vectors were classified as influx if the vector traveled over the ovariole image (left), or as efflux if the vector traveled away from the ovariole (right). Ion concentration gradients are shown as red gradients representing influx (left) or efflux (right).

flux were modified to include the diffusion coefficient for hydrogen (9.31×10^{-5} cm^{-2} s^{-1}), and the bath hydrogen concentration. 2-D and 3-D resultant vectors were generated from the *x*- and *y*-axes values and the *x*-, *y*- and *z*-axes values, respectively. The vertical *z*-axis data were excluded, because they confounded the data without contributing any essential further information.

Next, an image was generated using Adobe Illustrator™ 9.0 that displayed H^+ flux at each position measured along the ovariole, using the first image taken during the trial as a backdrop. The image corresponding to the vector being placed (showing the position of the probe in relation to the ovariole) was positioned over the original image and rendered partially transparent to allow the two ovariole images to be juxtaposed. If the second picture required rotating to line up correctly, as sometimes happened when the ovariole moved slightly during a trial, it was adjusted to the nearest 0.5°, and the corresponding vector was similarly rotated before being placed. A line of arbitrary, consistent length was scaled according to the vector magnitude, so that H^+ flux at different positions and from different ovarioles could be directly compared. Each vector was positioned so that the origin was next to the ovariole at the location where the probe measurement was taken. Once positioned, each vector was scored as a positive efflux if it extended away from the ovariole, or as a negative influx if it extended over the ovariole image.

Once signs had been assigned, the data from each ovariole were grouped according to ovariole stage, and stage-specific means and standard errors (S.E.M.) were calculated for each position measured along the ovariole. Using StatView software (SAS Institute Inc., Cary, NC, USA), single-factor analyses of variance (ANOVAs) were calculated for each stage, using ovariole position as the categorical variable, to assess the significance of signal vs. background noise. Significant difference was assigned as $P<0.05$. Fishers' PLSD (Protected Least Significant Differences) post-tests were performed to derive pairwise comparisons between all positions for each stage.

Results

General features of extracellular H^+ flux

When analyzing the main body of data we were interested in detecting both spatial differences in H^+ flux along the ovariole surface, and temporal differences occurring within an oogenesis cycle, i.e. by stage.

Significant extracellular H^+ fluxes were localized to specific ovariole structures. H^+ flux at some positions was especially prominent during all stages (Table 2), including all three positions along the interfollicular stalk separating the T and T-1 follicles, and both positions along the pedicel. In addition, H^+ flux at other positions became significant during later stages, notably the junction between T and T-1 follicles during stages 7–9, and the position where the anterior and posterior regions of the T follicle meet.

During the entire course of experimentation using ovarioles from insects dissected 3–12 d.p.f., only one stage-1 ovariole was encountered. This ovariole was unhealthy, and was consequently removed from subsequent analysis. Interestingly, only one of ten stage-3 ovarioles had formed a connective stalk long enough to measure three positions. During stage 4, H^+ efflux at the connective stalk separating T and T-1 follicles reached its maximum rate. By stage 5, all ovarioles sampled but one had well developed interfollicular stalks. Beginning with stage-7 ovarioles, a small but significant increase in H^+ efflux over the T-1 T-2 junction could be detected that was higher than other positions nearby. All other positions were not significantly different from background noise or from the positional average during previous stages. Along the T follicle in stage-8 ovarioles, H^+ flux at the anterior T 1/3 and 2/3 positions actually reversed to become a significant influx. Stage-9 ovarioles developed two strong H^+ effluxes not present in earlier stages. First, H^+ efflux was observed at the T-1:T-2 junction, anterior to the newly activated T-1 follicle. Weaker efflux in this region was observed during stages 7 and 8, and by stage 9 many T-1 follicles had entered vitellogenesis and formed well-developed interfollicular stalks. The stage-9 average was heavily weighted by trials with T-1 follicles in midvitellogenesis. H^+ efflux at the connective stalk separating T and T-1 follicles during stage 9 also increased. The second new H^+ flux was seen over the specialized rim and pseudomicropyle structures of the forming chorion. A strong, discretely localized efflux in this region was observed in two ovarioles. While the graphs presented here show only a single point, this efflux was characterized further, and is considered further below along with other special regions of interest.

The spatial and temporal patterns of H^+ fluxes presented in Table 2 are more easily visualized in a contour plot as (Fig. 3). Changes in H^+ flux along the anterior of the T follicle are evident, while pedicel H^+ fluxes were stable over time. Except for influxes along the anterior T 1/3 and 2/3 positions of stage-8 ovarioles (mentioned above), none of the influxes observed in later stages were significantly different from background noise.

Detailed analysis of H^+ flux at specific regions along the ovariole

The spatiotemporal patterns of extracellular H^+ flux, derived from the average flux at each position along ovarioles grouped according to stage, constitute the major focus of this work. In addition to the average extracellular fluxes observed, a few special cases not evident in the above data were encountered that merit discussion, and these are considered below.

During two scans of stage-9 ovarioles, an increased number of positions were measured near the prominent H^+ efflux near the forming chorion rim, in order to resolve the source of H^+ flux more accurately. H^+ efflux was confined to a narrow region along the horizontal (anteroposterior) *x–y* plane (Fig. 4), and continued circumferentially around the ovariole in the *z*-axis ($N=2$). In addition, H^+ efflux in this region could be

Table 2. *Mean extracellular H^+ flux at all positions along the adult* Rhodnius *ovariole*

	Developmental stage							
Ovariole position	2 (400–500 μm)	3 (500–600 μm)	4 (600–700 μm)	5 (700–800 μm)	6 (800–900 μm)	7 (900–1000 μm)	8 (1000–1500 μm)	9 (1500–2000 μm)
Noise	10±2 (10)	8±1 (10)	9±1 (9)	11±2 (10)	6±1 (12)	10±1 (10)	9±1 (17)	12±3 (10)
Troph tip	7±2 (10)	8±2 (10)	–1±3 (9)	10±4 (9)	6±4 (12)	7±3 (10)	4±4 (16)	15±4 (10)
Mid troph tip	0±4 (10)	1±4 (10)	–7±4 (9)	2±3 (9)	–2±3 (12)	–6±4 (10)	1±4 (17)	7±4 (10)
Ant troph	–1±5 (10)	2±5 (10)	–2±7 (9)	0±5 (9)	–7±5 (12)	2±6 (10)	–1±5 (17)	7±6 (10)
Ant troph 1/3	9±5 (10)	16±1 (10)	13±5 (9)	19±3 (10)	11±5 (12)	17±5 (10)	9±5 (17)	19±6 (10)
Ant troph 2/3	11±4 (10)	19±3 (10)	7±5 (9)	17±5 (10)	8±4 (12)	10±6 (10)	11±5 (17)	18±6 (10)
Troph widest	15±3 (10)	16±2 (10)	15±4 (9)	19±2 (10)	14±3 (12)	12±5 (10)	8±5 (17)	18±5 (10)
Post troph	10±4 (10)	14±1 (10)	9±4 (9)	15±2 (9)	7±6 (11)	3±5 (10)	10±5 (17)	11±7 (10)
Troph junction	7±8 (10)	21±6 (10)	9±6 (9)	16±7 (10)	9±7 (12)	5±7 (10)	20±18 (17)	26±10 (10)
Mid T-3	64±4 (2)	36±1 (2)	43±14 (3)	26±7 (7)	23±5 (10)	16±11 (10)	20±7 (16)	26±8 (10)
T-2:T-3 junction	44±7 (2)	30±8 (5)	18±3 (5)	26±8 (8)	25±8 (11)	13±6 (10)	18±6 (16)	25±10 (10)
Mid T-2	15±6 (10)	22±3 (10)	27±5 (9)	25±11 (10)	20±5 (12)	18±5 (10)	19±2 (17)	10±10 (10)
T-1:T-2 junction	42±27 (10)	21±3 (10)	27±9 (9)	33±7 (10)	28±9 (12)	**41±7** (10)	**41±12** (17)	**116±22** (10)
T-1 1/4	10±10 (6)	15±3 (10)	14±5 (9)	18±2 (9)	10±4 (12)	13±5 (10)	11±4 (17)	14±9 (10)
T-1 1/2	15±8 (10)	20±6 (10)	21±3 (9)	26±3 (10)	15±4 (12)	12±7 (10)	10±5 (17)	18±9 (10)
T-1 3/4	20±10 (6)	**44±8** (10)	39±7 (9)	41±6 (10)	25±6 (12)	21±8 (10)	15±5 (17)	14±11 (10)
Ant T stalk	49±2 (2)	**211** (1)	**174±57** (5)	**116±19** (9)	**60±17** (12)	45±12 (10)	29±7 (15)	48±23 (6)
Mid T stalk	**122±24** (10)	**202±30** (10)	**237±53** (9)	**181 ±29** (10)	**101±21** (12)	**74±18** (10)	**47±9** (17)	**149±23** (9)
Post T stalk	**172±67** (2)	**236** (1)	**316±55** (5)	**291±44** (9)	**146±26** (12)	**136±23** (10)	**86±11** (16)	**194±40** (9)
Ant T 1/3	43±13 (3)	**117±21** (10)	**145±44** (9)	**153 ±37** (10)	**66±23** (12)	16±33 (10)	**–38±20** (17)	32±26 (10)
Ant T 2/3	22±9 (3)	**47±10** (10)	49±24 (9)	**74±16** (10)	31±14 (12)	48±22 (10)	**–23±17** (17)	–25±18 (10)
Pseudomicropyle	–	–	82±14 (2)	**118** (1)	7±13 (2)	15±16 (2)	5±10 (5)	**271±4** (2)
T col/cub border	4±7 (3)	10±10 (10)	3±13 (9)	36±7 (10)	5±10 (11)	–8±10 (10)	**–25±11** (17)	–39±27 (4)
Lateral T 1/4	14±6 (10)	13±5 (10)	9±8 (9)	15±8 (10)	–8±9 (12)	–3±8 (10)	13±12 (16)	25±30 (10)
Lateral T 1/2	15±8 (10)	21±6 (10)	12±10 (9)	18±8 (10)	–2±9 (12)	–2±8 (10)	6±12 (17)	18±31 (10)
Lateral T 3/4	24±8 (10)	11±10 (10)	–8±19 (9)	7±8 (10)	–14±19 (12)	4±7 (10)	11±13 (17)	23±33 (10)
Post T corner	26±19 (3)	13±13 (10)	–1±15 (9)	34±10 (9)	–13±11 (12)	–9±9 (10)	8±11 (17)	47±32 (8)
Mid pedicel	**178±39** (9)	**246±23** (8)	**223±26** (9)	**190±20** (7)	**180±17** (10)	**202±20** (9)	**237±20** (10)	**208±10** (6)
Post pedicel	**120±32** (10)	**274±29** (9)	**235±48** (9)	**210±27** (10)	**198±24** (11)	**206±13** (9)	**244±29** (12)	**230±25** (6)
Thicker plug	–	**353** (1)	**245** (1)	**322±4** (2)	**270±4** (3)	**173±14** (3)	**295±18** (2)	–
Noise	10±2 (10)	10±1 (10)	9±1 (9)	10±2 (10)	12±1 (12)	10±1 (10)	10±5 (17)	14±2 (10)

Fluxes are presented in fmol cm^{-2} s^{-1} and are means ± S.E.M. Sample number is included in parenthesis. Values that differ significantly from the average noise measurements for each stage are in bold type.

detected along stage-9 T follicles held in different orientations, suggesting it formed a ring encircling the entire rim. Fine mapping of the region to identify individual cells responsible for generating H^+ efflux was not possible due to the limited optics of the side-mounted camera, and difficulties in visualizing specific groups of cells using the *xy*-plane camera due to the curvature of the ovariole. Nevertheless, the resolution was such that we could resolve a distinct and narrow zone (probably 3–4 cells wide at most) that composed part of the rim close to the juncture between the cap and the neck region of the main body (Fig. 4, asterisk). Remarkably, H^+ efflux in this area continued even after ovulation (*N*=2), when the associated chorionated oocyte had been released into the oviduct (Fig. 5, asterisk). No H^+ flux was detected around the corresponding region of a recently ovulated egg (*N*=1; not shown).

H^+ efflux begins at the junction between T-1 and T-2 follicles by stage 7, in the region of the newly forming connective (Fig. 6). Increased sampling in this region during four trials revealed that H^+ efflux also extended posteriorly,

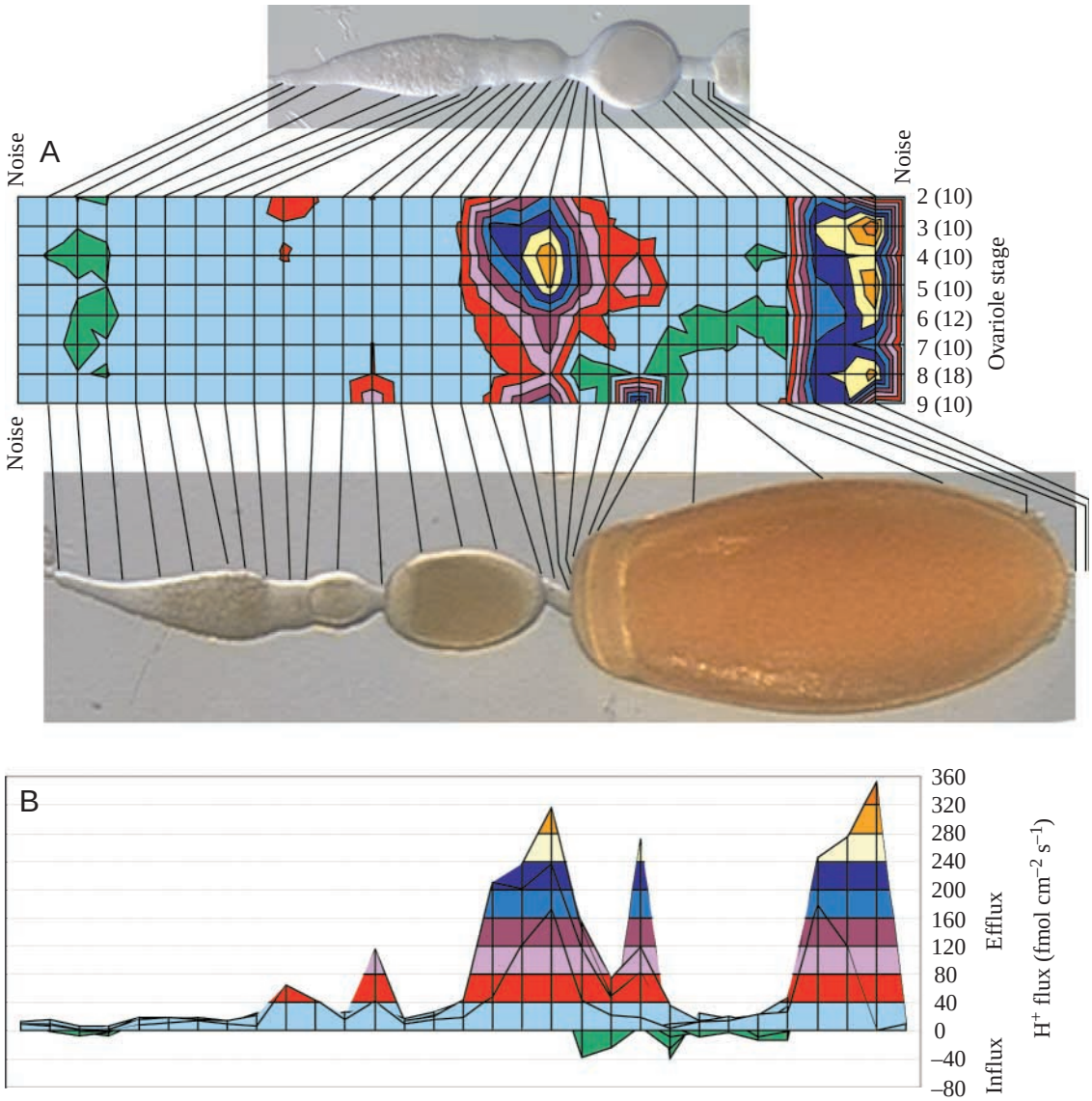

Fig. 3. Mean extracellular H^+ fluxes along adult *Rhodnius* ovarioles. (A) H^+ flux magnitude and direction (influx/efflux) relative to position along ovariole and ovariole stage (*N*=10–18, shown in parentheses). The data for each ovariole stage, represented by fluctuating black lines running through the coloured region of the plot, are superimposed on each other making it difficult to show stage differences. However these are clearly discerned in a top view as seen in (B). The colour coding indicates H^+ flux magnitude and direction, which is calibrated in B. Each vertical column on the surface plot corresponds to a specific point along the ovariole as indicated by the ovariole images. The leftmost column displays background noise. Horizontal rows display the average H^+ flux for each ovariole stage (see Materials and methods). Prominent efflux occurs near the interfollicular stalks on either side of the T follicle. H^+ efflux at the anterior stalk is greatest around stage 4 (early vitellogenesis) and declines gradually until stage 8 (late vitellogenesis) when it is significantly diminished. Stage-8 ovarioles were also characterized by the appearance of H^+ influx along the anterior columnar epithelium of the T follicle.

Fig. 4. Light micrograph of a stage-9 ovariole with corresponding extracellular H^+ fluxes superimposed. H^+ flux is indicated by red vectors, with length proportional to the flux magnitude. Vector angles are the result of summing *x*- and *y*- axis measurements. Vectors traveling away from the ovariole surface represent H^+ efflux; vectors traveling over the ovariole are influx. The noise measurement is in the bottom left corner. Of interest is the H^+ efflux near the forming chorion rim in late vitellogenic oocytes (asterisk), which remains throughout choriogenesis. Red scale bar, 100 fmol cm^{-2} s^{-1}; black scale bar, 100 µm.

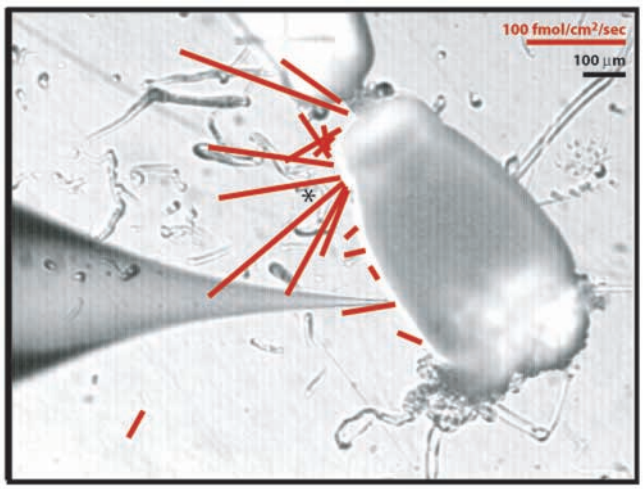

Fig. 5. Light micrograph of a recently ovulated follicle with corresponding extracellular H^+ fluxes superimposed. The chorionated oocyte was loosely contained by the follicular epithelium, and fell away from the ovariole during dissection. H^+ efflux in the region of the rim is still present after ovulation (asterisk), suggesting follicle cells generate this H^+ flux. Red scale bar, 100 fmol cm^{-2} s^{-1}; black scale bar, 100 µm.

presumably associated with the columnar follicle cells at the anterior pole of the oocyte (Fig. 6, asterisk).

Discussion

The foundation and blueprint for development is established during oogenesis through a complex orchestration of germ cells and numerous intra- and extraovarian somatic cell types. The discovery of dynamic, localized transmembrane H^+ fluxes in *Rhodnius* ovarioles coincident with regional cell differentiation and regulatory events suggests that these fluxes, along with associated changes or stabilization of pH_i, play a key role during oogenesis in the telotrophic ovariole. General aspects of the observed H^+ fluxes will be discussed before addressing specific localized and stage-related events, followed by consideration of the potential importance of these fluxes to changes occurring during oogenesis.

General features of extracellular H^+ flux during oogenesis in Rhodnius prolixus

One of the most striking features of H^+ flux around adult *Rhodnius* ovarioles is that the large, sustained transmembrane fluxes at the interfollicular stalk separating T and T-1 follicle and at the pedicel were effluxes. While average influxes were observed in other regions, notably the anterior tropharium and the anterior surface of the T follicle during stages 8–9, they were smaller and by no means balanced overall efflux. Substantial influxes were also observed during individual trials in regions that did not show average influxes, including over the lateral T follicle. As a result, H^+ flux across the cell membranes of the ovariole did not appear to add up to zero, suggesting that H^+ fluxes do not establish a current loop, but rather that an intracellular source produces H^+ for efflux.

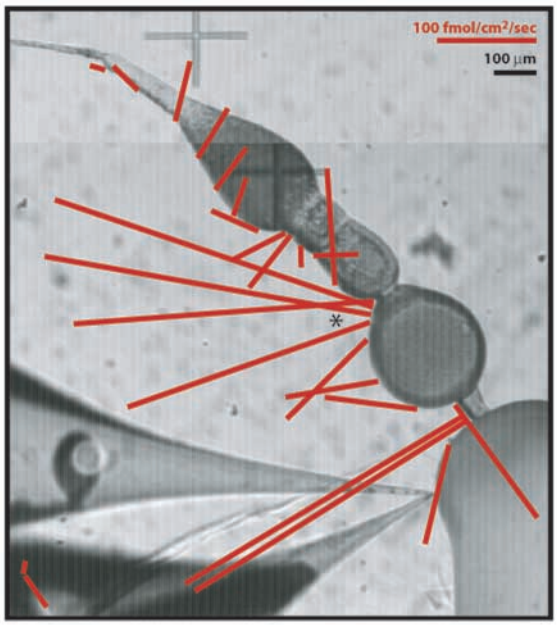

Fig. 6. Light micrograph of the anterior portion of a T-1 follicle from a stage-9 ovariole with corresponding extracellular H^+ fluxes superimposed. Additional measurements near the H^+ efflux along the T-1/T-2 junction reveal that the efflux extends to the anterior pole of the T-1 follicle (asterisk). These follicle cells presumably are also involved in interfollicular stalk morphogenesis, and will ultimately form the columnar cells at the anterior pole of the follicle. Red scale bar, 100 fmol cm^{-2} s^{-1}; black scale bar, 100 µm.

The lateral surfaces of vitellogenic T follicles did produce substantial H^+ fluxes; however, both influxes and effluxes were observed, and in calculating the mean values at each stage the balance of influx and efflux in these regions negated differences significant from noise. There are two possible explanations for these results: first, that the differences reflected the future embryonic axis, as shown for bioelectric currents around insect follicles (Bowdan and Kunkel, 1990) and that we were incapable of discriminating them, since T follicle orientation was not accounted for during these trials. A second possibility stems from the morphology of the lateral follicular epithelium, which forms large intercellular spaces during vitellogenesis to facilitate yolk uptake. The ion-selective probe may have been positioned over either the basal surface of a follicle cell or over the intercellular space. Differences in H^+ flux between these two regions, as might occur if small local current loops were established, might explain the measurements we obtained.

Regional H^+ fluxes observed during oogenesis

Prominent extracellular H^+ fluxes measured using the ion-selective probe were mapped to discrete regions of the ovariole, suggesting they are important to regional cell physiology. At many locations, the pattern of H^+ flux also changed over an oogenesis cycle, suggesting these temporal changes are linked to dynamic events during oogenesis. Thus it is important to consider the location and temporal dynamics of these fluxes relative to the germ and somatic cell events contributing to the development of a viable mature oocyte.

H^+ efflux at the junctions separating follicles

The interfollicular stalks are ideally situated to regulate interfollicular communication, coordinating entry into vitellogenesis or generating anteroposterior polarity in both adjoining follicles. Therefore, the prominent H^+ efflux observed at the interfollicular stalk separating T and T-1 follicles is significant. In particular, the stage-related variation in the strength of this H^+ efflux suggests a relationship to the development of the terminal follicle.

Oogenesis in insect ovarioles involves a progression of stages: an oocyte in the penultimate (T-1) position becomes the terminal oocyte once the current chorionated T follicle passes into the oviduct. The H^+ efflux at the anterior end of the T follicle could be traced back to follicles in the T-1 position as early as stage 7, where efflux begins before the connective stalk begins to form (see Fig. 6 and Results).

Identification of the cells that generate H^+ efflux will be essential to determine which cells might be affected by changes in pH_i, and will permit a better understanding of the potential downstream effects of H^+ efflux. Several cell groups exist at the junction separating T and T-1 follicles that could be wholly or partly responsible for generating the observed H^+ efflux (Fig. 7). For example, the somatic cells of the connective stalk are functionally isolated from the adjacent follicles. This could be seen when fluorescent dyes were injected into the oocytes of either follicle. The dyes moved into follicle cells surrounding the injected oocyte, but did not pass into cells of the stalk, or into adjacent follicles (see Fig. 7 for orientation). This suggested that stalk cells are not coupled to adjacent follicles *via* gap junctions (Huebner, 1981b; Telfer et al., 1982; E. Huebner, unpublished results). Thus transmembrane H^+ flux may influence intracellular H^+ levels in the cells forming the stalk, the follicle cells surrounding the oocyte, the oocyte itself, or some combination thereof. While the cells responsible for H^+ flux in this region cannot be positively identified by this study alone, we hope to address this question in future studies.

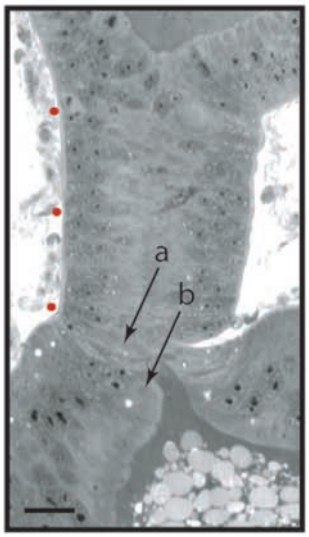

Fig. 7. Light micrograph of a longitudinal section through the interfollicular stalk separating T-1 (top) and T follicle (bottom). The ovariole sheath is still intact. The three positions measured along the stalk are shown as red dots, from anterior (top) to posterior (bottom). Two groups of cells are present near the posterior stalk position: the stalk cells which are not dye-coupled to either adjacent follicle (a), and follicle cells which are coupled to the T oocyte (b). Semi-thin section stained with 1% Toluidine Blue in 1% Borax. Scale bar, 20 μm.

H^+ influx along the anterior surface of the T follicle

A significant feature of stage-8 ovarioles was the onset of H^+ influx across the cap region of the T follicle. While H^+ influx was observed in some T follicles during earlier stages, it appears in the majority of follicles during stage 8 and early stage 9, when H^+ efflux at the connective stalk was reduced. Vitellogenesis is also occurring at a rapid pace during this period. Fusion of smaller yolk vesicles into larger, more membrane-efficient spheres requires acidification of the vesicle interior to release vitellogenin from its receptor (DiMario and Mahowald, 1986; Dittmann, 1997; Dittmann and Munz, 1999), so that excess membrane can be recycled to the oocyte surface. This process appears to involve H^+-pump activity, probably a V-ATPase (DiMario and Mahowald, 1986; O'Donnell and Sharda, 1994), or a Na^+/H^+ antiporter (Dittmann, 1997; Dittmann and Munz, 1999) to move H^+ from the ooplasm into the yolk spheres. It is possible that yolk vesicle acidification occurs during the later stages of oogenesis and is strong enough that it exhausts the H^+ pool available for efflux, so that cytoplasmic pH remains stable throughout vitellogenesis.

Strong H^+ efflux from follicle cells forming specialized chorion structures

While the source of other H^+ fluxes remains speculative, the H^+ efflux that develops during stage 9 near the cap rim, where the micropyle and pseudomicropyle cells form, is clearly generated by the follicle cells. H^+ efflux begins during

chorionation (Fig. 4), when most follicle cells are no longer coupled to the oocyte and are separated from it by the chorion. After the mature egg passed into the oviduct, H^+ efflux was still present along the follicle cells (Fig. 5) but not the egg (not shown), indicating the follicle cells generate this flux. H^+ efflux in this region occurs within a narrow zone and attenuates a short distance away in either direction along the anteroposterior axis (Fig. 4). While it was not possible to identify the exact group(s) of follicle cells responsible for generating this efflux, fine mapping of the region narrowed the field to a band of cells anterior to the neck, over the cells forming the rim.

It is unlikely that H^+ efflux here affects oocyte pH. Only one group of follicle cells remains in contact with the oocyte during choriogenesis, although it is unknown whether the cells remain electrically coupled. These cells are responsible for forming the micropyle, a channel in the shell allowing sperm to reach the oocyte. Typically, no more than 16 micropyle cells are present, with single cells or doublets spaced relatively evenly around the rim's circumference (Beament, 1946, 1947). These cells are neighbored by pseudomicropyle cells, which are similar in morphology, except the channels they form do not reach the oolemma. Approximately 200 of these cells circle the rim, which is about 250 μm in radius (Beament, 1946, 1947). This means that the micropyle cells are spaced roughly 11–12 cells, or 100 μm, apart. H^+ flux was measured for several tens of μm above and below the plane of measurement (not shown), without attenuating as it did along the anteroposterior axis. Since H^+ efflux in this region occurred around the entire rim and was not solely a product of the micropyle cells, it would appear that H^+ efflux in this region could not affect the oocyte. The link between these localized fluxes and their role in regional follicle cell differentiation merits further study (Huebner and Bjornsson, 2002).

Potential roles of transmembrane H^+ fluxes during oogenesis

The temporal and spatial pattern of transmembrane H^+ flux observed in this study underscores the potential importance of pH change in a number of cell differentiation and developmental events during oogenesis. A number of events during oogenesis in *Rhodnius* are potentially regulated by changes in pH_i; during the period when H^+ efflux was observed at the interfollicular stalk connecting T and T-1 follicles, gap-junctional coupling is established between follicle cells and the oocyte (Huebner and Injeyan, 1981), cytoskeletal changes occur in both oocyte and follicle cells (Watson and Huebner, 1986; McPherson and Huebner, 1993), and the oocyte engages in endocytic uptake of yolk precursors (Huebner and Anderson, 1972a,b). In this paper we establish the location and dynamic changes of extracellular H^+ fluxes generated by the adult *Rhodnius* ovariole during an oogenesis cycle, and consider a number of relevant pH-regulated events, the importance of which we hope to address in future studies. This research sets the stage for exploring a number of important questions regarding the role of H^+ dynamics in regulating oogenesis.

Discovery and Equipment grants to E.H. and postgraduate fellowships to C.B. from the Canadian Natural Sciences and Engineering Council are gratefully acknowledged. Technical support from Al Shipley (Applicable Electronics, Inc.) and Eric Karplus (Science Wares, Inc.) is greatly appreciated.

References

Anderson, K. L. and Woodruff, R. I. (2001). A gap junctionally transmitted epithelial cell signal regulates endocytic yolk uptake in *Oncopeltus fasciatus*. *Dev. Biol.* **239**, 68-78.

Beament, J. W. L. (1946). The formation and structure of the chorion of the egg in an hemipteran, *Rhodnius prolixus*. *Quart. J. Micr. Sci.* **87**, 393-437.

Beament, J. W. L. (1947). The formation and structure of the micropylar complex in the egg-shell of *Rhodnius prolixus* Stahl (Heteroptera Reduviidae). *J. Exp. Biol.* **23**, 213-233.

Bjornsson, C. S. and Huebner, E. (2002). Tissue rotation chamber for electrophysiology, microinjection, and microdissection. *Biotechniques* **33**, 38-42.

Bohrmann, J., Dorn, A., Sander, K. and Gutzeit, H. (1986). The extracellular electrical current pattern and its variability in vitellogenic *Drosophila* follicles. *J. Cell Sci.* **81**, 189-206.

Bohrmann, J. and Haas-Assenbaum, A. (1993). Gap junctions in ovarian follicles of *Drosophila melanogaster*: inhibition and promotion of dye-coupling between oocyte and follicle cells. *Cell Tissue Res.* **273**, 163-173.

Bowdan, E. and Kunkel, J. G. (1990). Patterns of ionic currents around the developing oocyte of the German cockroach, *Blattella germanica*. *Dev. Biol.* **137**, 266-275.

Bowdan, E. and Kunkel, J. G. (1994). Ionic components of dorsal and ventral currents in vitellogenic follicles of the cockroach, *Blattella germanica*. *J. Insect Physiol.* **40**, 323-331.

Busa, W. B. and Nuccitelli, R. (1984). Metabolic regulation via intracellular pH. *Am. J. Physiol.* **246**, R409-R438.

Diehl-Jones, W. L. and Huebner, E. (1989). Pattern and composition of ionic currents around ovarioles of the hemipteran, *Rhodnius prolixus* (Stahl). *Biol. Bull.* **176(S)**, 86-90.

Diehl-Jones, W. L. and Huebner, E. (1992). Spatial and temporal transcellular current patterns during oogenesis. *Dev. Biol.* **153**, 302-311.

Diehl-Jones, W. L. and Huebner, E. (1993). Ionic basis of bioelectric currents during oogenesis in an insect. *Dev. Biol.* **158**, 301-316.

DiMario, P. J. and Mahowald, A. P. (1986). The effects of pH and weak bases on the in vitro endocytosis of vitellogenin by oocytes of *Drosophila melanogaster*. *Cell Tissue Res.* **246**, 103-108.

Dittmann, F. (1997). The effect of ooplasmic pH regulation on the formation of yolk spheres in the telotrophic ovariole of *Dysdercus intermedius*. *J. Insect Physiol.* **43**, 189-195.

Dittmann, F., Ehni, R. and Engels, W. (1981). Bioelectric aspects of the hemipteran telotrophic ovariole (*Dysdercus intermedius*). *Roux's Arch. Dev. Biol.* **190**, 221-225.

Dittmann, F. and Munz, A. (1999). The proton/sodium antiporter (exchanger) in the oocyte membrane of *Dysdercus intermedius* is electrogenic ($2H^+/Na^+$) and causes perioocytic proton accumulation. *J. Insect Physiol.* **45**, 727-734.

Francis, D., Stergiopoulos, K., Ek-Vitorin, J. F., Cao, F. L., Taffet, S. M. and Delmar, M. (1999). Connexin diversity and gap junction regulation by pH_i. *Dev. Genet.* **24**, 123-136.

Gutzeit, H. O. (1986). Transport of molecules and organelles in meroistic ovarioles of insects. *Differentiation* **31**, 155-165.

Gutzeit, H. O. and Huebner, E. (1986). Comparison of microfilament patterns in nurse cells of different insects with polytrophic and telotrophic ovarioles. *J. Embryol. Exp. Morphol.* **93**, 291-301.

Haley, C. A. and O'Donnell, M. J. (1997). K^+ reabsorption by the lower Malphigian tubule of *Rhodnius prolixus*: inhibition by Ba^{2+} and blockers of H^+/K^+ ATPases. *J. Exp. Biol.* **200**, 139-147.

Harvey, W. R. and Wieczorek, H. (1997). Animal plasma membrane energization by chemiosmotic H^+ V-ATPases. *J. Exp. Biol.* **200**, 203-216.

Huebner, E. (1981a). Nurse cell-oocyte interaction in the telotrophic ovarioles of an insect, *Rhodnius prolixus*. *Tissue Cell* **13**, 105-125.

Huebner, E. (1981b). Oocyte-follicle cell interaction during normal oogenesis and atresia in an insect. *J. Ultrastruct. Res.* **74**, 95-104.

Huebner, E. (1984). The ultrastructure and development of the telotrophic

ovary. In *Insect Ultrastructure*, vol. 2 (ed. R. C. King and H. Akai), pp. 3-48. Plenum Press, New York.

Huebner, E. and Anderson, E. (1972a). A cytological study of the ovary of *Rhodnius prolixus*. I. The ontogeny of the follicular epithelium. *J. Morph.* **136**, 459-494.

Huebner, E. and Anderson, E. (1972b). A cytological study of the ovary of *Rhodnius prolixus*. II. Oocyte differentiation. *J. Morph.* **137**, 385-416.

Huebner, E. and Anderson, E. (1972c). A cytological study of the ovary of *Rhodnius prolixus*. III. Cytoarchitecture and development of the trophic chamber. *J. Morph.* **138**, 1-40.

Huebner, E. and Bjornsson, C. S. (2002). Follicle cell specialization during oogenesis: F-actin and ionic aspects. *Mol. Biol. Cell* (**2002 Suppl.**), 116a.

Huebner, E., Harrison, R. E. and Yeow, K. (1994). A new feeding technique for experimental and routing culturing of the insect, *Rhodnius prolixus*. *Can. J. Zool.* **72**, 2244-2247.

Huebner, E. and Injeyan, H. (1981). Follicular modulation during oocyte development in an insect: formation and modulation of septate and gap junctions. *Dev. Biol.* **83**, 101-113.

Huebner, E. and Sigurdson, W. J. (1986). Extracellular currents during insect oogenesis: special emphasis on telotrophic ovarioles. In *Ionic Currents in Development*, vol. 2 (ed. R. Nuccitelli), pp. 155-164. New York: Alan R. Liss Inc.

Jaffe, L. F. and Woodruff, R. I. (1979). Large electrical currents traverse developing *cecropia* follicles. *Proc. Natl. Acad. Sci. USA* **76**, 1328-1332.

Kuhtreiber, W. M. and Jaffe, L. F. (1990). Detection of extracellular calcium gradients with a calcium-specific vibrating electrode. *J. Cell Biol.* **110**, 1565-1574.

Kunkel, J. G. and Faszewski, E. (1995). Pattern of potassium ion and proton currents in the ovariole of the cockroach, *Periplaneta americana*, indicates future embryonic polarity. *Biol. Bull.* **189**, 197-198.

Lutz, D. A. and Huebner, E. (1980). Development and cellular differentiation of an insect telotrophic ovary (*Rhodnius prolixus*). *Tissue Cell* **12**, 773-794.

Lutz, D. A. and Huebner, E. (1981). Development of nurse cell-oocyte interactions in the insect telotrophic ovary (*Rhodnius prolixus*). *Tissue Cell* **13**, 321-335.

McPherson, S. M. G. and Huebner, E. (1993). Dynamics of the oocyte cortical cytoskeleton during oogenesis in *Rhodnius prolixus*. *Tissue Cell* **25**, 399-421.

Nordin, J. H., Beaudoin, E. L. and Liu, X. (1990). Coincident expression of the processing proteinase for an insect vitellin with acidification of yolk granules. *J. Cell Biol.* **111**, 485a.

Nordin, J. H., Beaudoin, E. L. and Liu, X. (1991). Acidification of yolk granules in *Blattella germanica* eggs coincident with proteolytic processing of vitellin. *Arch. Insect Biochem. Physiol.* **18**, 177-192.

O'Donnell, M. J. (1985). Calcium action potentials in the developing oocytes of an insect, *Rhodnius prolixus*. *J. Exp. Biol.* **119**, 287-300.

O'Donnell, M. J. and Sharda, R. K. (1994). Membrane potential and pH regulation in vitellogenic follicles of an insect, *Rhodnius prolixus*. *Physiol. Zool.* **67**, 7-28.

Overall, R. and Jaffe, L. F. (1985). Patterns of ionic current through *Drosophila* follicles and eggs. *Dev. Biol.* **108**, 102-119.

Perrachia, C. and Perrachia, L. L. (1980). Gap junction dynamics: reversible effects of hydrogen ions. *J. Cell Biol.* **87**, 719-727.

Pratt, G. E. and Davey, K. G. (1972). The corpus allatum and oogenesis in *Rhodnius prolixus* (Stahl). I. The effects of allatectomy. *J. Exp. Biol.* **56**, 201-214.

Regula, C. S., Pfeiffer, J. R. and Berlin, R. D. (1981). Microtubule assembly and disassembly at alkaline pH. *J. Cell Biol.* **89**, 45-53.

Schatten, G., Bestor, T., Balczon, R., Henson, J. and Schatten, H. (1985). Intracellular pH shift leads to microtubule assembly and microtubule-mediated motility during sea urchin fertilization: correlations between elevated intracellular pH and microtubule activity and depressed intracellular pH and microtubule disassembly. *Eur. J. Cell Biol.* **36**, 116-127.

Somieski, P. and Nagel, W. (2001). Measurement of pH gradients using an ion-sensitive vibrating probe technique (IP). *Pflugers Arch. Eur. J. Physiol.* **442**, 142-149.

Southwick, F. S. (2000). Gelsolin and ADF/cofilin enhance the actin dynamics of motile cells. *Proc. Natl. Acad. Sci. USA* **97**, 6936-6938.

Telfer, W. H. (1965). The mechanism and control of yolk formation. *Annu. Rev. Entomol.* **10**, 161-184.

Telfer, W. H. (1975). Development and physiology of the oocyte-nurse cell syncytium. *Adv. Insect Physiol.* **11**, 223-319.

Telfer, W. H., Woodruff, R. I. and Huebner, E. (1981). Electrical polarity and cellular differentiation in insect meroistic ovaries. *Am. Zool.* **21**, 675-686.

Telfer, W. H., Huebner, E. and Smith, D. S. (1982). The cell biology of vitellogenic follicles in *Hyalophora* and *Rhodnius*. In *Insect Ultrastructure*, vol. 1 (ed. R. C. King and H. Akai), pp. 118-149. New York, Plenum Press.

Tilney, L. G., Kiehart, D. P., Sardet, C. and Tilney, M. (1978). Polymerization of actin IV. Role of Ca^{++} and H^{+} in the assembly of actin and in membrane fusion in the acrosomal reaction of echinoderm sperm. *J. Cell Biol.* **77**, 536-550.

Vanderberg, J. P. (1963). Synthesis and transfer of DNA, RNA, and protein during oogenesis in *Rhodnius prolixus* (Hemiptera). *Biol. Bull.* **125**, 556-575.

Verachtert, B. and DeLoof, A. (1986). Electric currents around the polytrophic ovarian follicles of *Sarcophaga bullata* and the panoistic follicles of *Locusta migratoria*. In *Ionic Currents in Development* (ed. R. Nuccitelli), pp. 173-180. New York: A. R. Liss.

Watson, A. J. and Huebner, E. (1986). Modulation of cytoskeletal organization during insect follicle cell morphogenesis. *Tissue Cell* **18**, 741-752.

Woodruff, R. I., Huebner, E. and Telfer, W. H. (1986a). Electrical properties of insect ovarian follicles: some challenges of a multicellular system. In *Ion Currents in Development* (ed. R. Nuccitelli), pp. 147-154. New York, AR Liss.

Woodruff, R. I., Huebner, E. and Telfer, W. H. (1986b). Ion currents in *Hyalophora* ovaries: the role of the epithelium and the intercellular spaces of the trophic cap. *Dev. Biol.* **117**, 405-416.

Woodruff, R. I. and Telfer, W. H. (1990). Activation of a new physiological state at the onset of vitellogenesis in *Hyalophora* follicles. *Dev. Biol.* **138**, 410-420.

Woodruff, R. I. and Telfer, W. H. (2002). Ion physiology of vitellogenic follicles. *J. Insect Physiol.* **48**, 915-923.